Progress In Electromagnetics Research C, Vol. 132, 159–170, 2023

Realization of Broadband Negative Refractive Index in Terahertz Band by Multilayer Fishnet Metamaterial Approach

Sudarshan Kalel[1] and Wei-Chih Wang[1, 2, 3, 4, *]

Abstract—In the present study, a broad negative refractive index (NRI) performance is achieved in the terahertz frequency range (0.6–0.9 THz) through the design of multi-layered fishnet metamaterial (FMM). Herein, the conventional fishnet structure is modified by smoothing the sharp corners to reduce the electric field concentration and improve NRI. At corner radius, $r = 30\,\mu$m, an effective refractive index of -11.14 is achieved with lower electric field concentration at the corners. A multilayer structure of up to 40 layers is studied to achieve a broad NRI frequency response. The frequency band of NRI response is improved from 0.034 THz for a single layer structure to 0.178 THz for 28 layer structure, almost 6 times the original bandwidth. With the increase in the number of layers, the improvement in NRI and Figure of Merit (FOM) is observed, and maximum NRI and FOM values of -87.5 and 12.67 are achieved at 28 layers. This multilayer broadband design can surpass tunable response of available electro-optic materials. With an optimal combination of NRI and FOM, the presented multilayer approach can achieve a low-loss, broadband performance.

1. INTRODUCTION

For the last two decades, the negative refractive index (NRI) has fascinated and motivated researchers to develop technologies and devices that are simpler and more efficient for the current fast-paced world. Applications like perfect lens [1, 2] and invisible cloak [3] are made possible with these NRI materials. In the real world, many applications demand stable and efficient performance of devices over a wide frequency range. The wavelength-dependent refractive index of optical materials is a major limitation to develop broadband optical devices. A uniform refractive index over wide frequency band can allow researchers to extend phenomena like superlens and cloaking to broader wavelengths. To obtain the NRI response over broad frequency, special geometries and multilayer structures have been used by researchers [4–11]; however, these structures have limitations which will be discussed ahead. A special nano-scale split ring type resonator was used by Atre et al. [4] to show broad 250 nm wavelength range, NRI ($n' = -1.9$) in visible and near-infrared regions. A polarization independent 2 layered metamaterial that exhibits NRI in microwave region with a refractive index of -2.66 at 14.19 GHz and 0.51 GHz range was studied by Aydin et al. [12]. Another broadband NRI plasmonic metamaterial by the combination of cut wires and dimers exhibited approximately 10% of bandwidth around 14.4 GHz frequency [9]. Horizontal and vertical hyperbolic stacking of metal-dielectric layers [6, 13], optically [7], and thermally [14] tunable approaches have also been studied to develop broadband NRI structures. Recently, terahertz waves have also shown great potential in communications, imaging and security [15–17], sensors [18, 19], and energy harvesting [20, 21] applications. In the terahertz range, a broad response of almost 0.5 THz (from 0.4 THz to 0.9 THz) was achieved by thermally tuning the substrate

Received 23 February 2023, Accepted 23 April 2023, Scheduled 28 April 2023

* Corresponding author: Wei-Chih Wang (abong@uw.edu).

[1] Institute of Nanoengineering and Microsystems, National Tsinghua University, Hsinchu City, Taiwan. [2] Power Mechanical Engineering, National Tsinghua University, Hsinchu City, Taiwan. [3] Department of Mechanical Engineering, University of Washington, Seattle, WA, USA. [4] Department of Electrical & Computer Engineering, University of Washington, Seattle, WA, USA.

material [14]. However, this structure shows NRI response only under the influence of heat. Apart from this, many reported structures in the terahertz region are single/dual narrow bands or require special designs that are complicated to fabricate [22, 23]. In this work, we attempt to broaden the resonance of a single-layer fishnet structure by stacking a number of fishnet-shaped metal and dielectric layers and utilize multiple resonances to broaden the NRI response. The goal is to develop broadband NRI metamaterial with a simple geometry that is easy to fabricate and works at room temperature. By using such structures, a flat perfect lens (considering NRI response) based on a multi-layer array of subwavelength cells with broadband performance could be realized.

We particularly select PVDF-TrFE-CTFE (terpolymer) material that has the potential to make the device tunable, so the tunability response can be compared to the broadband response of the proposed design. Since, to apply the electric potential, the materials need metal electrodes on both sides, it is a suitable candidate to become the Metal-Insulator-Metal (MIM) structure. In our work, first, we design a simple fishnet structure with resonance frequency between 0.6 and 0.9 THz, then modify this structure by smoothing the sharp corners to reduce electric field concentration and improve NRI response. Second, we design a multi-layered fishnet structure to achieve broad NRI and low loss. The effect of the number of layers on transmission, refractive index, figure of merit (FOM), and absorbance is studied. Some optimum operating conditions concerning FOM and refractive index are suggested in discussion section.

2. METHODOLOGY

We begin the design process by first performing experiments to measure the refractive index and extinction coefficient of PVDF terpolymer in the range of 0.2–1 THz because there is no information currently available. THz time domain system (THz-TDS) (Batop Optoelectronics) is used to derive these properties from S_{21} measurement. The results are plotted in Supplementary data Fig. 1. From measured 'n' and 'k,' real and imaginary parts of permittivity are calculated by using relations $\varepsilon' = n^2 - k^2$, $\varepsilon'' = 2nk$. Silver is used as metal layer with Drude's model having plasma frequency equal to 14.602×10^{15} rad/s and collision frequency equal to 13.5×10^{12}/s. All the numerical simulations are done using commercially available SIMULIA CST Studio Suite 2022. Periodic boundary conditions are applied to a unit cell along X and Y directions during the simulation with the assumption of an infinite metamaterial array, where wave travels in the $-Z$ direction. To simulate a 3×3 array, $E_t = 0$ at $+Y$ and $-Y$ directions; and $H_t = 0$ at $+X$ and $-X$ are applied as boundary conditions.

Estimating the complex refractive index, permittivity, and permeability from S-parameters is a well-established method that has been described by earlier researchers [24–27]. To begin, the complex impedance 'z' is estimated from S_{11} and S_{21} parameters,

$$z = \pm\sqrt{\frac{(1+S_{11})^2 - S_{21}^2}{(1-S_{11})^2 - S_{21}^2}} \tag{1}$$

$$r = \frac{(z-1)}{(z+1)} \tag{2}$$

$$n = \frac{1}{k_0 d}\left\{\mathrm{Im}\left(\ln\left|\frac{1-rS_{11}}{S_{21}}\right|\right) + 2m\pi - i\mathrm{Re}\left(\ln\left|\frac{1-rS_{11}}{S_{21}}\right|\right)\right\} \tag{3}$$

where k_0 is the wavevector; d is the effective medium thickness; m is the branch due to the periodicity of function and is considered as 0 [25].

Afterwards, permittivity (ε) and permeability (μ) are calculated from n and z.

$$\varepsilon = \frac{n}{z} \tag{4}$$

$$\mu = nz \tag{5}$$

3. RESULTS AND DISCUSSION

First, we designed a conventional fishnet structure to exhibit double-negative (DNG) response around 0.72 THz and compared its performance with modified (rounded corner) fishnet structure in the aspect

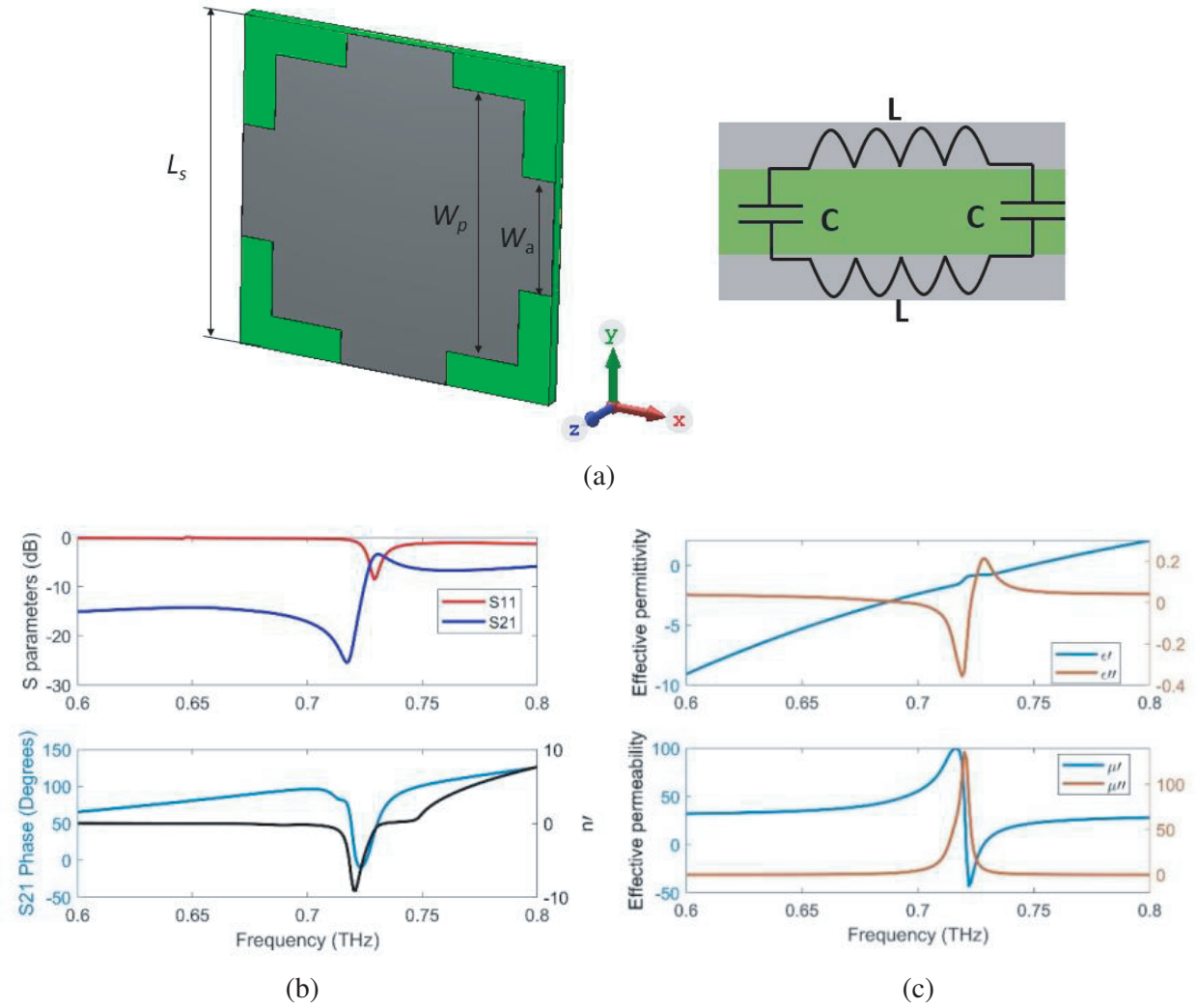

Figure 1. (a) Fishnet unit cell and equivalent LC circuit (Green and grey colour represent dielectric and metal respectively). (b) Simulated results of S parameters for unit cell (resonance near 0.72 THz), S_{21} phase, and real part of estimated refractive index. (c) Estimated effective permittivity and permeability of unit cell FMM structure showing double negative performance.

of NRI. Furthermore, the multilayer structure with optimized corner radius is studied for different numbers of layers to achieve broad NRI with lower losses. The conventional fishnet design is shown in Fig. 1(a). The total length of the unit cell (L_s) is 220 µm; patch width (W_p) is 175 µm; arm width (W_a) is 75 µm whereas the thickness of substrate (t_s) and metal (t_m) is 15 µm and 0.1 µm, respectively.

S parameters, S_{21} phase, and estimated real part of refractive index (n') are shown in Fig. 1(b). The phase shift here is more than $\pi/2$ at the resonance where the refractive index is equal to -9.1 at 0.72 THz. Fig. 1(c) depicts the effective permittivity and permeability of the fishnet structure, evaluated from (4) and (5). Near the resonance, a double negative effect (minimum ε' of ~ -1 and μ' of ~ -43) is achieved.

We performed smoothing of the sharp corners of conventional FMM by adding radius at the corners. The motive here is to reduce the electric field concentration at the corners and reduce difficulties that arise during the fabrication process to achieve such sharp corners [28]. The effect of different corner radii on the impedance and refractive index is plotted in Fig. 2. Due to the rounded corners, the impedance is reduced, with a lower concentration of electric charges on the surface during resonance. Fig. 3(a) shows the electric field distribution on the surface of the fishnet cell (at the interface of air and

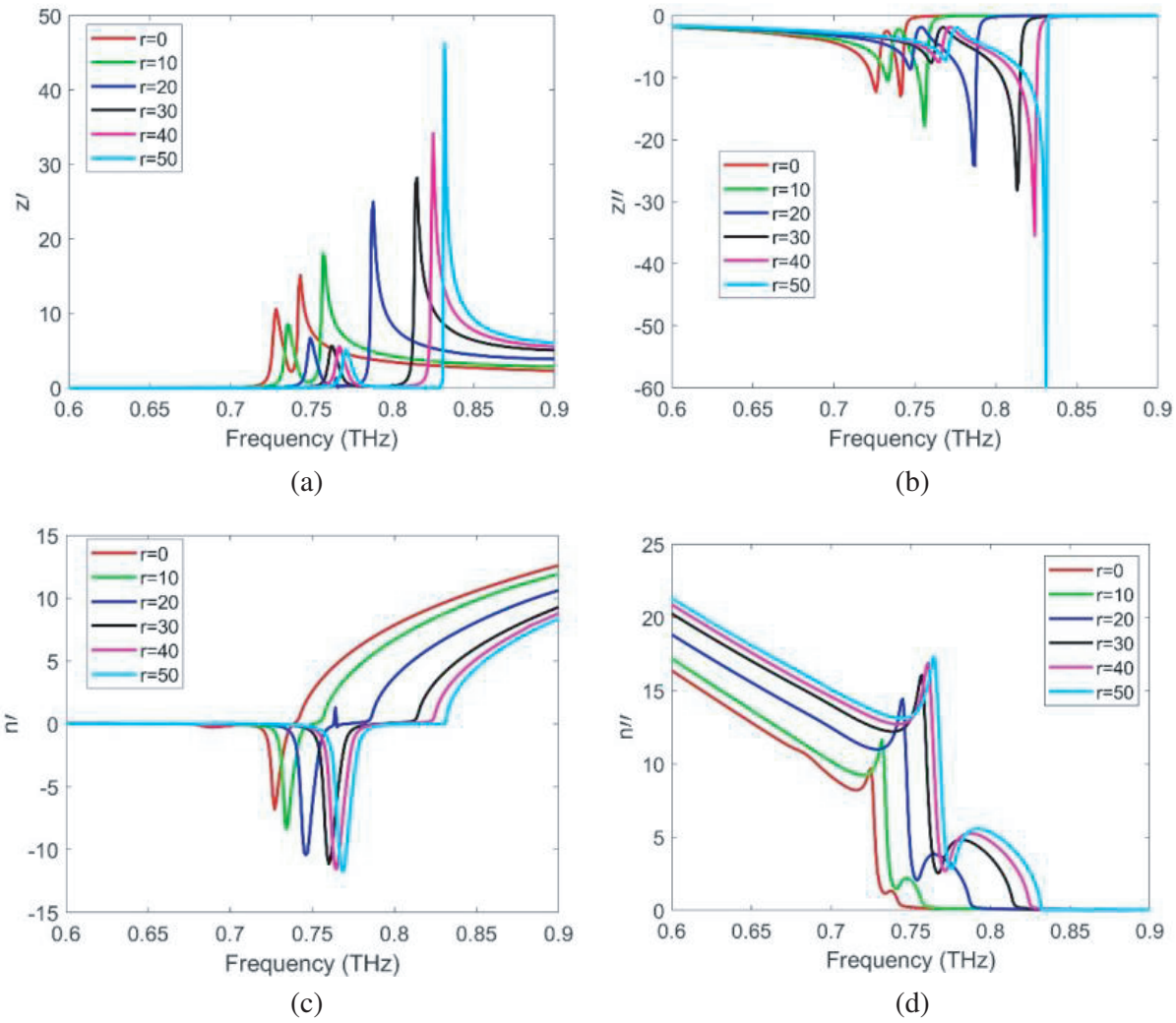

Figure 2. Modified FMM study. Effect of corner radius (in μm) on the (a) real and (b) imaginary part of the impedance, and (c), (d) refractive index.

metal layer) for sharp and rounded corners at resonance on the same scale. The E-field concentration at the corner decreases with an increase in radius. It is easy to notice that after 30 μm, the maximum E-field concentration at the corners and n' saturates. Here, impedance is given as $Z \propto \sqrt{L/C}$ (L *and* C are inductance and capacitance, respectively). If the input field (V) is the same, and charge concentration (Q) decreases, then C decreases (as $CV = Q$), and impedance will increase. However, there is an increase in the rotating field along the thickness of the fishnet structure with the addition of corner radius, as depicted in Fig. 3(b) (observing the color and size of arrows), meaning that the inductance that opposes the current flowing through the structure is reduced. This field increases up to $r = 30\,\mu$m and saturates afterwards. With the reduction in inductance, the impedance decreases. The reduction in inductance must be dominating the increase in capacitance, due to which there is a decrease in impedance with the increase in corner radius.

Since $\omega = \sqrt{1/LC}$, due to the reduction in L and C, the resonance frequency shifts toward a higher value. As presented in (3), the estimation of refractive index totally depends on the magnitude and phase of S-parameters, as well as impedance characteristics. Hence, due to the combined effect of these parameters, with an increase in radius, $-n'$ increases, with resonance shifting toward a higher frequency. At 0.76 THz for $r = 30\,\mu$m, n' is -11.43 compared to the index of sharp cornered structure (-9.1 at 0.72 THz) along with lower concentration E-field. Meanwhile, after 30 μm, the shape of the

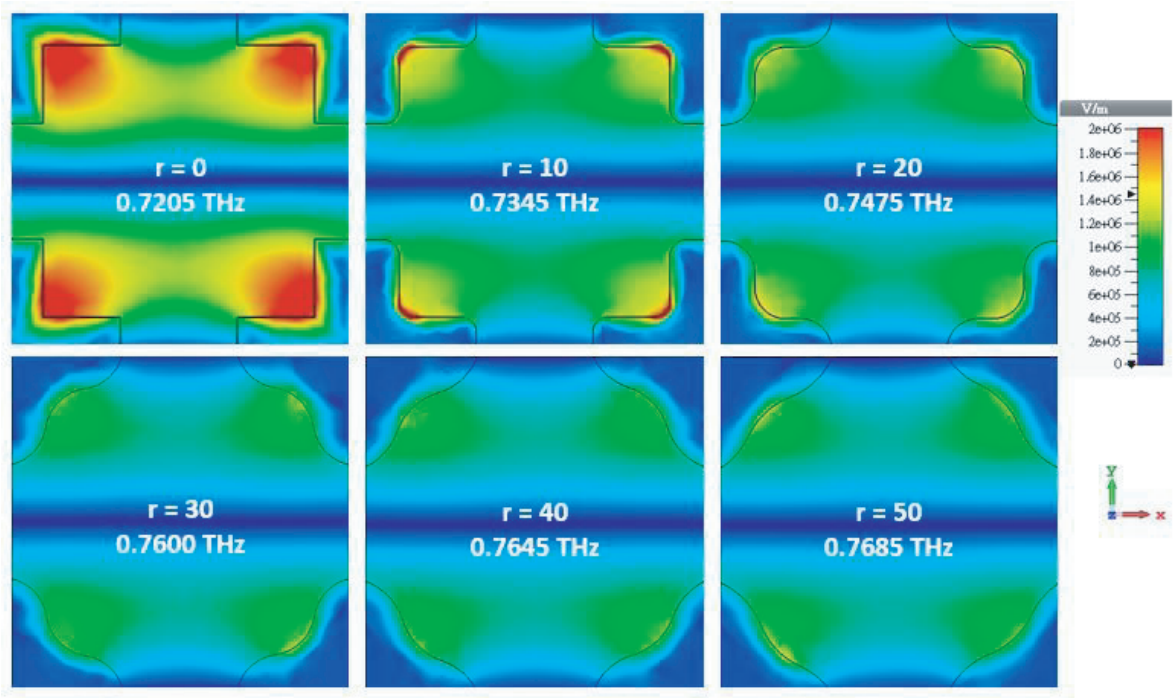

(a)

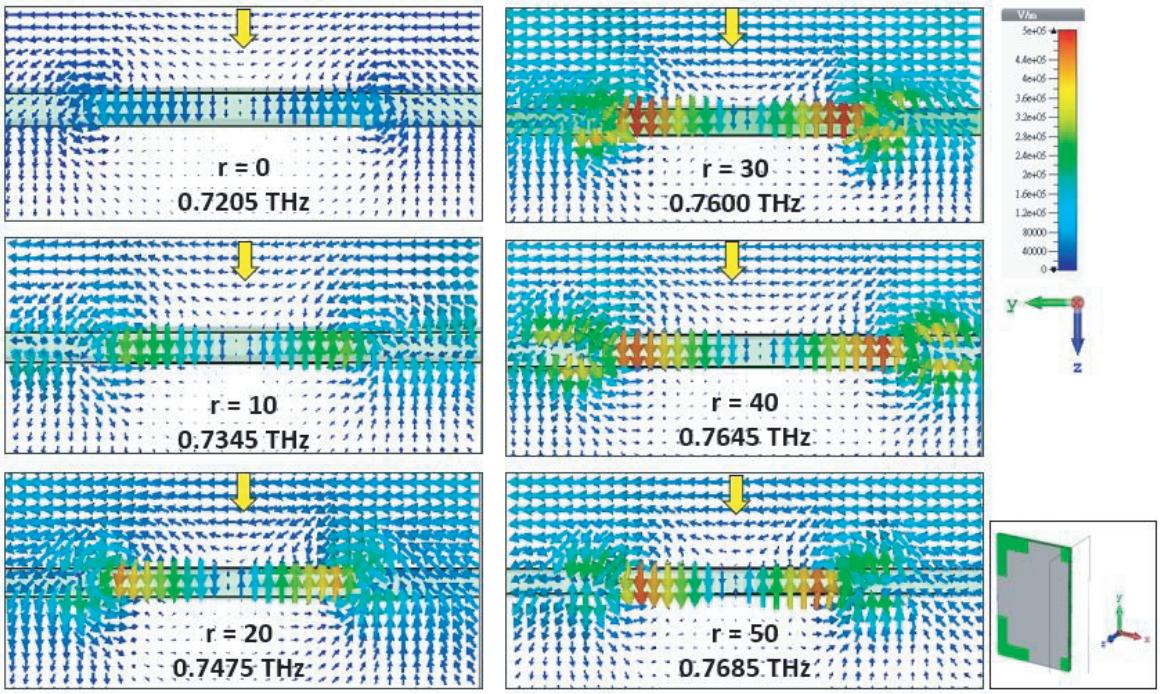

(b)

Figure 3. Modified FMM study. (a) E-field distribution on the surface of fishnet cell at different corner radii (frequency mentioned corresponds to minimum n'). All the plots presented on same scale. (b) E-Field Vector plot along the thickness of structure. All the plots are presented on same scale. Yellow arrow shows the direction of wave propagation, cutting plane (YZ) is depicted in bottom right corner.

square patch is disrupted. Therefore, for all further studies, fishnet cell with $r = 30\,\mu m$ is considered.

One might argue just using a circular patch fishnet instead of just rounding the corners. However, we compared our patch design with $r = 30\,\mu m$ to a circular patch keeping the arm width and patch size similar as shown in Fig. 4(a). No resonance is seen within the given range due to which no NRI response is exhibited by circular patch fishnet design. However, the resonance exhibited by an equivalent circular fishnet structure lies at frequency more than 1 THz (please refer to Figs. 2–4 in supplementary data). Furthermore, to compare the left-handed material (LHM) response of the FMM unit cell with a finite array, a 3×3 single layer (m-d-m) array is modelled. The estimated n' for unit cell and array shows remarkably close performance as shown in Fig. 4(b).

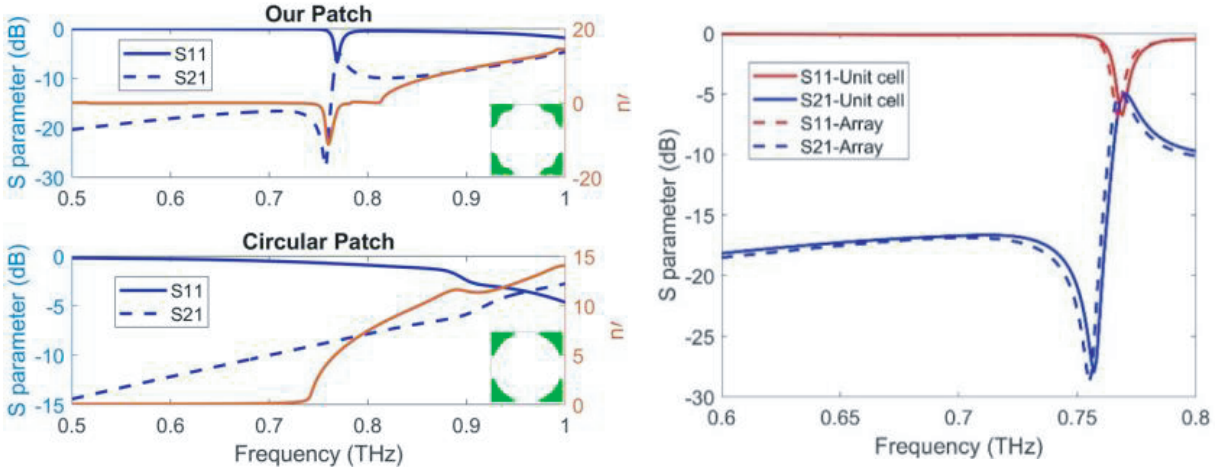

Figure 4. (a) S parameters and n' comparison between our rounded cornered fishnet patch ($r = 30\,\mu m$) and circular patch. (b) S parameters for FMM unit cell vs 3×3 single layer finite array of the rounded cornered design.

The multilayer structure is modelled by stacking numbers of a fishnet-shaped metal layer (m) and a dielectric layer (d) without any air gap between them. Here, single layer means m-d-m; 2 layers mean m-d-m-d-m, and so on. A structure up to 40 layers is numerically simulated and estimated, and results of transmission loss, impedance, refractive index, and FOM are plotted for the different numbers of layers. Here FOM is defined as the ratio of real to imaginary part (n'/n'') of estimated refractive index. The normalized S_{21} parameter or transmission (where $T = |S_{21}|^2$) for the multilayer structure is plotted in Fig. 5. Just before the resonance, S_{21} is extremely low for structures with more than one layer. For a single layer, maximum S_{21} is $\sim 60\%$ at the resonance, and it further decreases with the addition of layers. The dispersive behaviour of polymer material and multiple reflections between metal electrodes could be major factors reducing the transmission of light through the structure [6, 28].

It can be observed that the resonance peak is broadened instead of a sudden jump in the S_{21} curve with the addition of layers. As seen from Fig. 5, a single peak in the S_{21} curve of 1 layer structure is transformed into multiple peaks at the resonance, contributed by each layer in the structure. These multiple peaks broaden the frequency response with a reduction in the amplitude of light transmission. A similar broadband response is expected in the S_{21} phase curve. As the values of refractive indices are estimated through amplitude and phase of S parameters, the ultimate effect is seen in the n' curve due to broad anomalous dispersion (Fig. 6(a)). Table 1 summarizes the estimated results for multilayer structure, $\min n'$ (or $\max -n'$ for our understanding) and corresponding frequency (f_{nr}), frequency range within which $-n'$ occurs (Δf_{nr}), max. FOM (where FOM $= n'/n$"), and n' at the frequency corresponding to max. FOM (f_{FM}). Maximum NRI band Δf_{nr} of ~ 0.18 THz ($\sim 24\%$) is achieved at 28 layers, 6 times as compared to single layer FMM.

Here, the value of NRI is also improved from -11.14 for a single layer to -87.5 for 28 layers' structure. Our approach to estimation is purely based on the employment of the finite element method

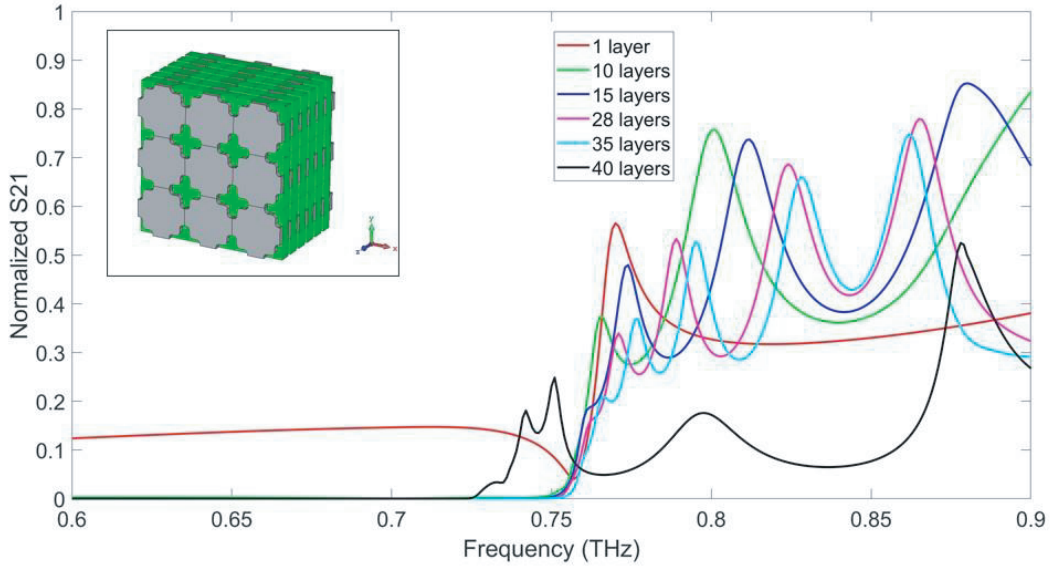

Figure 5. Effect of the number of layers on transmission through the structure. Inset shows the modified multilayer fishnet metamaterial.

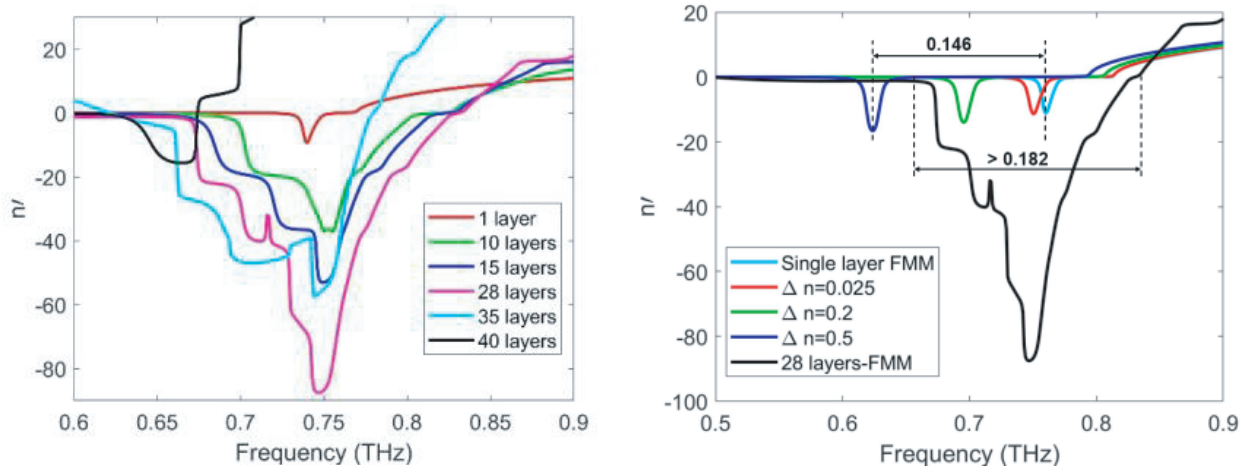

Figure 6. (a) Estimated n' for different layers. (b) Comparing tunable design vs current broadband design.

for S-parameter retrieval expressed by (1)–(3). Herein, along with multiple resonances due to the multilayer structure, the effective thickness (d) of the structure in (3) also increases with the addition of layers. This d is inversely proportional to the effective refractive index and is calculated by adding thicknesses of the number of substrate and metal layers. With an increase in the number of layers, we observe that this effective thickness for the 28-layered structure becomes almost equal to the wavelength corresponding to $\sim$ 0.75 THz, due to which the constructive effect of these layers might provide a greater n'. For 35 layers, this effective thickness is not close to the resonance wavelength, and the n' value starts diminishing. In the same way, the 40-layered structure should have a lower n' than the 35-layer structure; however, the sudden reversal of sign before 0.7 THz might indicate an estimation error in the computation. According to the effective medium theory (EMT), the estimated effective

Table 1. Summary of results.

No. of layers	Min n' and corresponding frequency (f_{nr}) in THz	Range of $-n'$ (Δf_{nr}) in THz (% of f_{nr})	Max. FOM within Δf_{nr} and corresponding frequency (f_{FM})	n' at f_{FM}
1	−11.14 @ 0.760	0.034 (4.47)	2.16 @ 0.764	−7.19
10	−37.73 @ 0.755	0.114 (19.07)	9.98 @ 0.785	−9.25
15	−53.03 @ 0.749	0.175 (23.36)	10.53 @ 0.790	−12.92
28	−87.51 @ 0.747	0.178 (23.82)	12.67 @ 0.780	−30.62
35	−57.8 @ 0.744	0.157 (21.10)	4.03 @ 0.762	−17.38
40	−15.62 @ 0.665	0.060 (9.09)	< 0.1	−15.62

refractive index should be independent of thickness in the direction of propagation of electromagnetic (EM) waves [24]. A recent work by Liu et al. [29] demonstrated the limitations of EMT in estimating effective parameters for multilayer metamaterials. They observed significant discrepancies between EMT and the Finite Element Method (FEM) results for multilayer structures, with the deviation increasing with the number of layers. Additionally, the presence of low spacing between metallic layers (dielectric thickness) contributes to this error, as EMT does not account for the coupling between these layers. Consequently, the reliability of the S-parameter retrieval method for estimating effective parameters in multilayer structures with multiple resonance phenomena may be questioned. Despite these limitations, the goal of this study was to showcase broadband negative refractive index (NRI), and the multilayer approach employed herein demonstrates such performance.

The selected electro-active PVDF terpolymer substrate could serve the tunable response, as the reported change in refractive index (Δn) due to the applied electric field is equal to 0.025 in the 3–5 μm wavelength range [30]. For now, we assume the same Δn of PVDF terpolymer substrate to check its frequency shift in the THz region. In addition, we also use Δn change up to 0.2 in THz region, as electro-optic material like liquid crystal can exhibit such Δn change [28]. We also consider a non-realistic farfetched $\Delta n = 0.5$ for the sake of comparison of frequency response with our multilayer structure. Fig. 6(b) depicts comparison in the shift of estimated n' due to Δn equal to 0.025, 0.2, and 0.5, respectively. As shown, the maximum shift due to $0.5\Delta n$ is ~ 0.146. As shown, the maximum shift due to $0.5\,\Delta n$ is 0:146; however, 28-layered structure exhibits a broad response of more than 0.182 THz that surpasses the frequency response of all the Δn. Hence, this approach can eliminate the use of external aid or active materials to achieve negative index in wider frequency ranges.

The quality of performance of the structure is usually measured by FOM, and an ideal structure shows a high value of FOM meaning a lower loss in the structure. Maximum FOM achieved within the NRI band increases with a greater number of layers. For 28 layers FOM is 12.67, and with further addition of layers FOM decreases (as shown in Fig. 7(a)). For 40 layers this FOM value drops to less than 0.1. Extremely high loss in the material with the addition of layers is responsible for such behaviour. In Table 1, all the frequencies corresponding to maximum FOM (f_{FM}) are higher than 0.76 THz. For 28 layers, the max. FOM occurs at 0.780 THz, whereas NRI at this frequency is −30.62. Hence, this structure can be operated around the frequency corresponding to max. FOM to exhibit NRI. As listed in Table 1, the optimum conditions for structures with different layers can be achieved to obtain NRI with reasonable FOM.

Figure 7(b) represents the absorbance in multilayer metamaterial, herein absorption coefficient is calculated by $A(\omega) = 1 - T(\omega) - R(\omega)$, where ω represents the frequency. $T(\omega)$ and $R(\omega)$ are transmission and reflection coefficients respectively and are estimated from S-parameters, i.e., $T = |S_{21}|^2$ and $R = |S_{11}|^2$. The estimated absorbance increases within 0.74–0.77 THz for all the layers. The maximum absorbance for 28 layers is close to single layer structure near the resonance. Hence, maintaining the same loss in the structure better NRI and FOM values are achieved.

Table 2 compares different metamaterial structures and their broadband performances in the

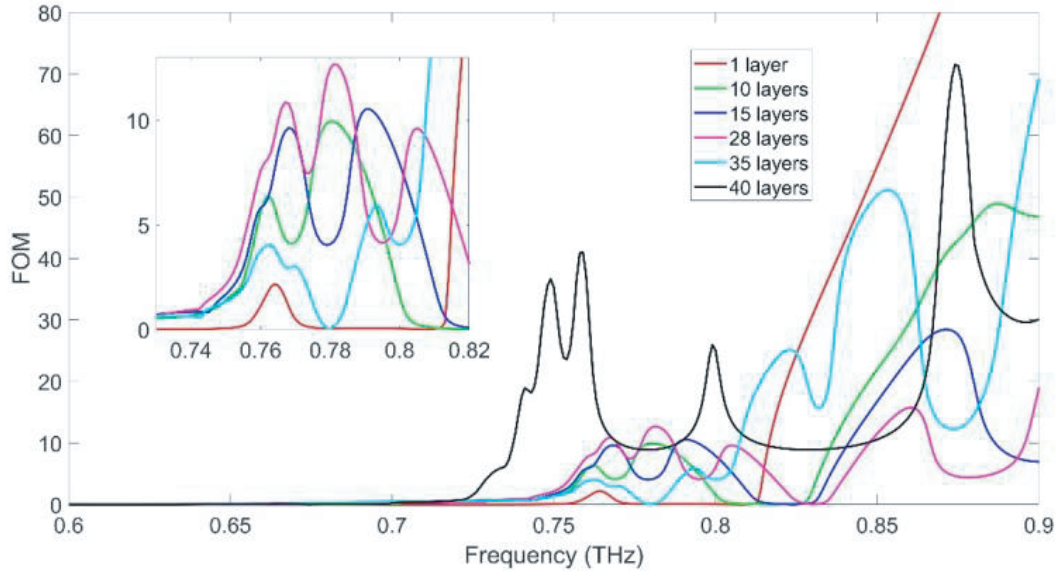

(a)

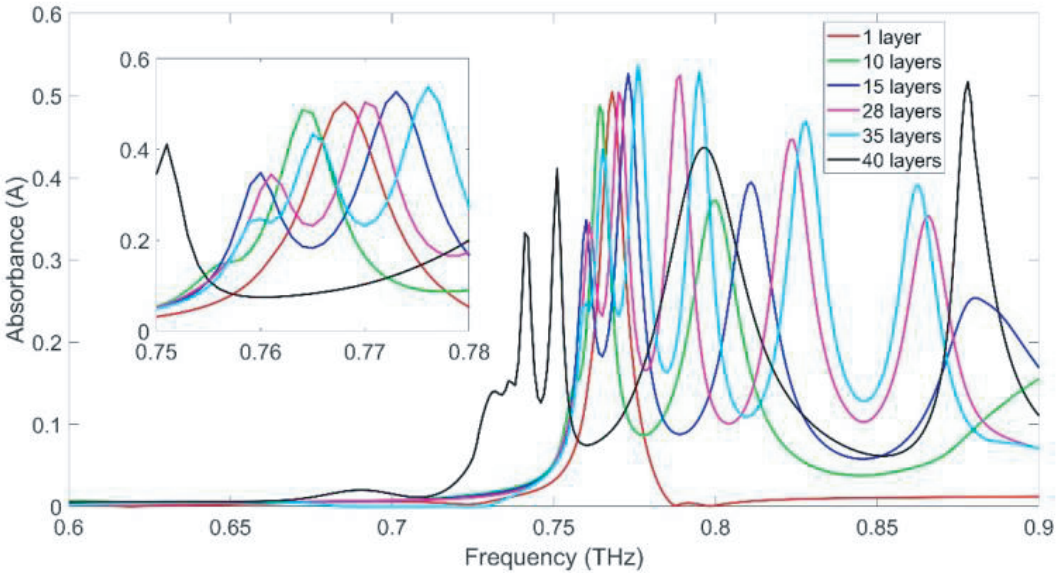

(b)

Figure 7. (a) Effect of addition of layers on FOM. (b) Absorbance in the structure with different number of layers.

terahertz regime. In the case of [7], a 3D Split Ring Resonator (SRR) is inserted within the polyimide substrate, and VO_2 is used in the gap between the top and bottom layers. Herein by tuning the VO_2 through temperature control, a tunable broadband metamaterial is achieved. However, such a structure requires special materials like VO_2, and the performance of the structure deteriorates at room temperature. The work of [14, 31] demands the fabrication of vertically standing structures that are complicated to fabricate. Zhang et al. [32] depicted dual band NRI response in the THz range with a SiO_2 substrate. However, all these studies consider a dispersion-free dielectric or semiconductor substrate material which can be questionable in terms of its accuracy and reliability of the results. In contrast, we attempted to measure the dispersive properties of substrate material in the desired frequency region. The achieved refractive index is also much higher than others' work. Our recent work [33] highlights the

Table 2. Comparison among different broadband NRI THz metamaterials.

Geometry	Unit cell size (μm)	NRI frequency range (THz)	Minimum n' obtained within the range	NRI bandwidth (THz)
Symmetrical 3D SRRs [7]	70×70	1.3–2.9	−9	1.6
Vertical L-shaped metal [14]	80×80	0.4–0.9, 1.06–1.14	−6	0.5, 0.09
Plasmonic fishnet [32]	64×64	2.04–2.42, 3.12–3.28	−9	0.38, 0.16
Planer metallic outer L shape and inner ring [31]	20×20	3.08–3.64, 4.10–4.37	−7	0.56, 0.27
Current work (28 layers)	225×225	0.65–0.83	−87.5	0.18

issues related to a sudden jump, known as a 'modulo jump', in the transmission phase and the estimated dielectric properties of metamaterials due to incorrect selection of the 'm' branch of a sinusoidal function. Such a 'modulo jump' can be observed in the estimated properties reported by [7, 14]. However, the FMM studied in this work does not exhibit any sudden jump in the phase or refractive index, as shown in Fig. 1(c). The current approach requires no special or expensive materials like graphene or VO_2, or external energy to realize a broad NRI response. The broadband performance also dominates the tunable response of naturally available materials. The current multilayer structure provides a simple reliable way to generate a broadband performance in the terahertz region by properly optimizing the rounding of the corners of the square patch and stacking them in layers with appropriate thickness.

4. CONCLUSION

By modifying sharp corners of the conventional fishnet, the enhancement in NRI with the reduction in E-field concentration can be achieved. By multilayer approach the NRI band is improved from 0.034 THz for a single layer to ~ 0.18 THz for 28 layers, almost 6 times of the original bandwidth. A minimum NRI of −87.5 and a maximum FOM of 12.67 are achieved within the broad NRI response at 28 layers. Such a multilayer structure can be operated with optimal NRI and FOM values to achieve better performance in the given range. The current multilayer design can surpass the tunable response of the many electro-optic materials. Such NRI broadband structures can help to realize applications like flat lenses in different frequencies.

ACKNOWLEDGMENT

This work was supported by Ministry of Science and Technology, Taiwan (MOST 107-2221-E-007-054-MY3, 111-2221-E-007-001 and MOST 111-2221-E-007-101).

REFERENCES

1. Pendry J. B., "Negative refraction makes a perfect lens," *Physical Review Letters*, Vol. 85, No. 18, 3966–3969, 2000.
2. Parimi, P. V., W. T. Lu, P. Vodo, and S. Sridhar, "Imaging by flat lens using negative refraction," *Nature*, Vol. 426, No. 6965, 404–404, 2003.
3. Cai, W., U. K. Chettiar, A. V. Kildishev, and V. M. Shalaev, "Optical cloaking with metamaterials," *Nature Photonics*, Vol. 1, No. 4, 224–227, 2007.
4. Atre, A. C., A. García-Etxarri, H. Alaeian, and J. A. Dionne, "A broadband negative index metamaterial at optical frequencies," *Advanced Optical Materials*, Vol. 1, No. 4, 327–333, 2013.

5. Bang, S., S. So, and J. Rho, "Realization of broadband negative refraction in visible range using vertically stacked hyperbolic metamaterials," *Scientific Reports*, Vol. 9, No. 1, 14093, 2019
6. García-Meca, C., J. Hurtado, J. Martí, A. Martínez, W. Dickson, and A. V. Zayats, "Low-loss multilayered metamaterial exhibiting a negative index of refraction at visible wavelengths," *Physical Review Letters*, Vol. 106, No. 6, 067402, 2011.
7. Ling, F., Z. Zhong, R. Huang, and B. Zhang, "A broadband tunable terahertz negative refractive index metamaterial,", *Scientific Reports*, Vol. 8, No. 1, 9843, 2018.
8. Ling, F., Z. Zhong, Y. Zhang, R. Huang, and B. Zhang, "Broadband negative-refractive index terahertz metamaterial with optically tunable equivalent-energy level,", *Optics Express*, Vol. 26, No. 23, 30085–30099, 2018.
9. Nguyen, H. T., T. S. Bui, S. Yan, G. A. E. Vandenbosch, P. Lievens, L. D. Vu, and E. Janssens, "Broadband negative refractive index obtained by plasmonic hybridization in metamaterials," *Applied Physics Letters*, Vol. 109, No. 22, 221902, 2016.
10. Rasad, A., H. T. Yudistira, F. Qalbina, A. G. Saputro, and A. Faisal, "Multilayer flexible metamaterials based on circular shape with negative refractive index at microwave spectrum," *Sensors and Actuators A: Physical*, Vol. 332, 113208, 2021.
11. Zhu, C., C.-H. Liang, and L. Li, 'Broadband negative index metamaterials with low-loss," *AEU — International Journal of Electronics and Communications*, Vol. 65, No. 9, 724–727, 2011.
12. Aydin, K., Z. Li, L. Sahin, and E. Ozbay, "Negative phase advance in polarization independent, multi-layer negative-index metamaterials," *Optics Express*, Vol. 16, No. 12, 8835–8844, 2008.
13. Cho, H., Y. Yang, D. Lee, S. So, and J. Rho, "Experimental demonstration of broadband negative refraction at visible frequencies by critical layer thickness analysis in a vertical hyperbolic metamaterial,", *Nanophotonics*, Vol. 10, No. 15, 3871–3877, 2021.
14. Li, W., Q. Meng, R. Huang, Z. Zhong, and B. Zhang, "Thermally tunable broadband terahertz metamaterials with negative refractive index," *Optics Communications*, Vol. 412, 85–89, 2018.
15. Cooper, K. B., R. J. Dengler, N. Llombart, B. Thomas, G. Chattopadhyay, and P. H. Siegel, "THz imaging radar for standoff personnel screening," *IEEE Transactions on Terahertz Science and Technology*, Vol. 1, No. 1, 169–182, 2011.
16. Ferguson, B. and X.-C. Zhang, "Materials for terahertz science and technology," *Nature Materials*, Vol. 1, No. 1, 26–33, 2002.
17. Muthuramalingam, K. and W.-C. Wang, "Non-destructive evaluation of the medical device packages using the terahertz time-domain spectroscopy," *SPIE Smart Structures + Nondestructive Evaluation*, Vol. 12048, SPIE, 2022.
18. Cheng, Y. T., Y. H. Chiang, C. Y. Kao, H. H. Chen, and W. C. Wang, "THz gas detection using cellulose nanoporous foam," *2018 43rd International Conference on Infrared, Millimeter, and Terahertz Waves (IRMMW-THz)*, 2018.
19. Davies, A. G., A. D. Burnett, W. Fan, E. H. Linfield, and J. E. Cunningham, "Terahertz spectroscopy of explosives and drugs," *Materials Today*, Vol. 11, No. 3, 18–26, 2008.
20. Wang, W.-C. and P. Garu, "Design of an ultra-wideband omnidirectional and polarization insensitive flower petal antenna for potential ambient electromagnetic energy harvesting applications," *Scientific Reports*, Vol. 12, No. 1, 6096, 2022.
21. Lin, H.-R. and W.-C. Wang, "Midinfrared radiation energy harvesting device,", *Journal of Photonics for Energy*, Vol. 3, 038001, 2017.
22. Du, Q.-J., J.-S. Liu, K.-J. Wang, X.-N. Yi, and H.-W. Yang, "Dual-Band Terahertz Left-Handed Metamaterial with Fishnet Structure," *Chinese Physics Letters*, Vol. 28, No. 1, 014201, 2011.
23. Wongkasem, N., A. Akyurtlu, J. Li, A. Tibolt, Z. Kang, and W. Goodhue, "Novel broadband terahertz negative refractive index metamaterials: Analysis and experiment," *Progress In Electromagnetics Research*, Vol. 64, 205–218, 2006.
24. Chen, X., T. M. Grzegorczyk, B.-I. Wu, J. Pacheco, and J. A. Kong, "Robust method to retrieve the constitutive effective parameters of metamaterials," *Physical Review E*, Vol. 70, No. 1, 016608, 2004.

25. Numan, A. B. and M. S. Sharawi, "Extraction of material parameters for metamaterials using a full-wave simulator [Education Column]," *IEEE Antennas and Propagation Magazine*, Vol. 55, No. 5, 202–211, 2013.
26. Hsieh, F.-J. and W.-C. Wang, "Full extraction methods to retrieve effective refractive index and parameters of a bianisotropic metamaterial based on material dispersion models," *Journal of Applied Physics*, Vol. 112, No. 6, 064907, 2012.
27. Ghodgaonkar, D. K., V. V. Varadan, and V. K. Varadan, "Free-space measurement of complex permittivity and complex permeability of magnetic materials at microwave frequencies," *IEEE Transactions on Instrumentation and Measurement*, Vol. 39, No. 2, 387–394, 1990.
28. Chang, C.-L., W.-C. Wang, H.-R. Lin, F. J. Hsieh, Y.-B. Pun, and C.-H. Chan, "Tunable terahertz fishnet metamaterial," *Applied Physics Letters*, Vol. 102, No. 15, 151903, 2013.
29. Liu, T., S. Ma, B. Yang, S. Xiao, and L. Zhou, "Effective-medium theory for multilayer metamaterials: Role of near-field corrections," *Physical Review B*, Vol. 102, No. 17, 174208, 2020.
30. Jeong, D.-Y., Y. K. Wang, M. Huang, Q. M. Zhang, G. J. Kavarnos, and F. Bauer, "Electro-optical response of the ferroelectric relaxor poly (vinylidene fluoride-trifluoroethylene-chlorofluoroethylene) terpolymer,", *Journal of Applied Physics*, Vol. 96, No. 1, 316–319, 2004.
31. Mishu, S. J., R. A. K. Moushi, N. Dhar, and M. A. Rahman "Design of a dual-band terahertz planar double-negative metamaterial with near zero refractive index property," *2021 International Conference on Science & Contemporary Technologies (ICSCT)*, 2021.
32. Zhang, S., Z. Wei, L. Xu, J. Xu, S. Ouyang, and Y. Shen, "Plasmonic fishnet structures for dual band THz left-handed metamaterials," *Photonics*, Vol. 8, No. 4, 116, 2021.
33. Wegrowski, A., W.-C. Wang, and C. Tsui, "Three cases of discontinuous refractive index in metamaterial study," *Scientific Reports*, Vol. 12, No. 1, 3558, 2022.